American International Journal of Research in Science, Technology, Engineering & Mathematics

Available online at http://www.iasir.net

ISSN (Print): 2328-3491, ISSN (Online): 2328-3580, ISSN (CD-ROM): 2328-3629

AIJRSTEM is a refereed, indexed, peer-reviewed, multidisciplinary and open access journal published by International Association of Scientific Innovation and Research (IASIR), USA
(An Association Unifying the Sciences, Engineering, and Applied Research)

Microstructural characterization of bead on welding of austenitic 202 grade stainless steel using shielded metal arc welding

[1]Apurv Choubey and [2]Vijay Kumar S. Jatti
[1]Assistant Professor, [2]Assistant Professor,
Symbiosis Institute of Technology (SIT),
Symbiosis International University (SIU),
Lavale, Pune-412 115, Maharashtra, INDIA

***Abstract**: Austenitic stainless steels are engineering materials which contain 18% Cr–8% Ni. Due to their striking blend of excellent mechanical properties, formability, and corrosion resistance.They find wide range of applications in industries, namely chemical industries and beverage manufacturing. In this study the effect of welding heat input on the bead height, bead width, depth of penetration and micro structural changes in the weldment had been evaluated. Experimental results showed that the bead height and depth of penetration is greatly affected by heat input and both increases as heat input increases. Full penetration welds were obtained in all the three combinations of heat input. Fusion zone and HAZ area increases as heat input increase. From the optical micrographs it is seen that as heat input increases the dendrite size and inter dendritic spacing in the weld metal also increase.*

***Keywords**: Austenitic steel; Weldment characteristics; Heat affected zone; Heat input; Welding parameters*

I. Introduction

Austenitic stainless steels (ASS) are the most favored construction material for various components required in chemical, petrochemical, fertilizer and nuclear industries because of its good combination of corrosion resistance and mechanical properties [1-2]. Austenitic stainless steels are broadly categorized in to 300-Series and 200-Series [2]. AISI 304 stainless steel is a family member of 300 series and widely used in most of the important applications like, fabrication of pressure vessel, nuclear reactor and other components [2]. Their chemical composition, mechanical properties, weldability and corrosion/oxidation resistance provide the best all-round performance stainless steels at relatively low cost [2]. They have excellent low temperature properties and respond well to hardening by cold working. The carefully controlled chemical composition of the Cr-Mn austenitics enables them to be deep drawn without intermediate annealing. This has made them dominant in the manufacture of drawn stainless steel parts such as sinks and saucepans. They are readily press-braked or roll formed into a variety of shapes for applications in the industrial, architectural and transportation fields [3-4]. 200 series which are mainly includes manganese, chromium, nitrogen and small amount of nickel. Both grades contain in excess of 12 % chromium for corrosion resistance and should therefore have similar atmospheric corrosion properties [2]. The primary difference in chemical composition is the alloy additions used to achieve an austenitic condition at room temperature. Type 304 utilizes nickel in the range of 8-12% as an austenite stabilizer. Type 200 utilizes less nickel (3.5-5.5%) and substitutes increased manganese (5.5-7.5%), also an austenite stabilizer, to achieve this condition. Nickel prices have been relatively high over the last couple of years. As a result, there has been increased interest in low-nickel or no-nickel grades of 200 series stainless steel. Since the two grades are austenitic grades with comparable chromium content in excess of 12%, the corrosion resistance of the two grades would be expected to similar. Chromium content is the primary factor in corrosion resistance of stainless steels. Viano et al. [5] investigated the effect of heat input and travel speed on microstructural characteristics and mechanical properties of welds in 20 mm thickness high strength low alloy steel HSLA 80, of Australian manufacture. They found that as the heat input is increased, the cooling rate decreased resulting in a larger cellular dendritic cell spacing, decreased acicular ferrite content, and coarser acicular ferrite laths. The effect of travel speed on delta ferrite cell spacing and prior austenite grain size was found to be co-dependent on the heat input and the thermal profile resulting from multiple electrodes welding. Prasad and Dwivedi [6] investigated the influence of the submerged arc welding (SAW) process parameters on the microstructure, hardness, and toughness of HSLA steel weld joints. Results showed that the increase in heat input coarsens the grain structure both in the weld metal and heat affected zone (HAZ). The hardness has been found to vary from the weld centre line to base metal and peak hardness was found in the HAZ. Prasad et al. [7] describes the effect of heat input on the microstructure and tensile properties of high strength low alloy steel weldments produced by submerged arc

welding. Results showed that the increase in the heat input affects the proportions of different micro-constituents both in the weld metal and heat affected zone. It is observed that the tensile strength (UTS, YS) decreases with increase in heat input and scanning electron microscopy of tensile test fractured surfaces usually exhibited ductile failure. Viano et al. [8] showed an micro-structural analysis and mechanical properties of welds in 20 mm thickness high strength low alloy steel HSLA 80 and specimens were prepared using the double tandem (four wire) submerged arc welding process in which both heat input and travel speed were varied. The inclusion size distribution was determined for selected welds and showed that heat input had a major effect. Karthik et al. [9] studied the weldability properties of the shielded metal arc welded and welded and tungsten inert gas welded austenitic 304 stainless. Both the process showed the tensile strength below the base metal value but the TIG welding better fracture strength than SMAW. Sathiya et al. [10] studied the bead-on -plate welds on AISI 904 L super austenitic stainless steel sheets using gas metal arc welding process. From the experimental results, the gray relational analysis is applied to optimize the input parameters simultaneously considering multiple output variables. In order to understand the micro-structural changes occurring in the weld zone is investigated through the optical microscopy. The hardness measurements were taken across the fusion zone. Kianersi et al. [11] optimized welding parameters namely welding current and time in resistance spot welding (RSW) of the austenitic stainless steel sheets grade AISI 316L. Then the effect of optimum welding parameters on the resistance spot welding properties and microstructure of AISI 316L austenitic stainless steel sheets has been investigated. It can be concluded that the bead geometry and penetration affect the weldment characteristics and are dependent on welding process parameters. In the present investigation an attempt was made to study weldment characteristics such as bead height, bead width & depth of penetration and micro structural changes in weldment, as affected by heat input (controlled by welding current, welding voltage and welding speed).

II. Experimental Details

The base material used in the present investigation was in the form of 202 SS plates of sizes 150 mm X 75 mm X 3mm which were cut using wire-cut electrical discharge machine from a rolled sheet and the filler was "AWS E308L-16" solid electrode of 3.15 mm diameter. Table I shows the chemical composition of the base and the filler used.

Table I Chemical composition

Elements	Base material (202 SS)	Filler material (AWS E308L)
Cr	13.34	18.00
Ni	0.2087	9.00
C	0.27	0.04
Mn	9.84	0.80
Si	0.460	0.90
S	0.0105	0.03
P	0.0693	0.04

In the present work double V-groove design was used so that welding could be accomplished ensuring full penetration. Before welding all the edges were thoroughly cleaned in order to avoid any source of contamination like rust, scale, dust, oil, moisture that could creep into the weld metal and later on could result possibly into a weld defect. Bead-on-plate SMAW was performed along the centre line of solution annealed plates using electrode "AWS E308L-16" of diameter 3.15 mm. The samples were denoted by A, B, C as shown in Fig. 1. Sample A of (75 A, 100 A, 125 A) were then ethched chemically in order to see the penetration macroscopically as well as to take optical microstructures of welded area. Sample B of (75 A, 100 A, 125 A) were polished at various grit papers and after cloth polishing micro-hardness were performed perpendicularly along weld pool, HAZ region and base metal. Sample C of (75 A, 100 A, 125 A) were used. After tacking the plates together the weld pass was given using SMAW process with welding conditions as mentioned in Table II. Although SMAW process was used in the manual mode, still utmost care was taken during recording of the arc on time so as to facilitate calculations of heat input. It is worth mentioning here that the best welding practice available in the fabrication industry was used in the present work. It is a well established fact that among all the welding variables in arc welding processes welding current is the most influential variable since it affects the current density and thus the melting rate of the filler as well as the base material. A rest time of 30 seconds was allowed after every subsequent pass.

Heat input was calculated according to equation 1:

$$H = \frac{\eta * V * I}{v} \quad (1)$$

where, H= heat input in KJ/mm, η= efficiency = 0.75 for SMAW, V= voltage in volts, I= current in amperes, v= welding speed in mm/sec.

So in accordance with this fundamental fact three different heat input combinations corresponding to different welding currents i.e. 75 A (low heat input), 100 A (medium heat input) and 125 A (high heat input) combinations were selected for the present study.

Figure 1 Bead-on-plate SMAW

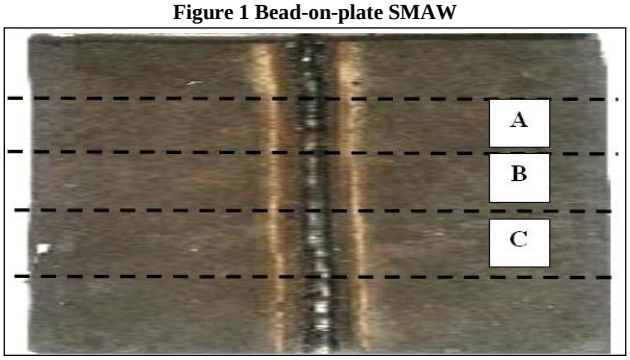

The reason for using these specific welding current values was twofold firstly, this spectrum of heat input combinations results in arc energies which are sufficient to cause adequate fusion of the base and weld metal selected for the present study and secondly, a step increase of 25 A was anticipated to be sufficient enough to cause a direct and significant influence on the microstructure and tensile properties of the welded joints. During and after welding the joints were visually inspected for their quality and it was ensured that all weld beads possessed good geometrical consistency and were free from visible defects like surface porosity, blow holes etc.

Table II Welding process parameters

Voltage (V)	Current (A)	Welding Speed (mm/sec)	Heat Input (KJ/mm)
35	75	2.50	0.787
35	100	2.50	1.050
35	125	2.50	1.312

III. Results and Discussions

In order to observe the micro-structural changes that take place during welding, corresponding to each heat input combination; specimens were machined out from the weld pads. After polishing and macro etching the cross sections of the joints were captured with the help of image analysis software coupled with a stereo zoom microscope at a magnification of 100X to facilitate measuring of the details like cross sectional areas of the fusion zone and HAZ. Standard polishing procedures were used for general micro-structural observations. Microstructures of different zones of interest like weld metal, HAZ and fusion boundary under different heat input combinations were viewed and captured with an optical microscope (Zeiss Axiolab) coupled with an image analyzing software. The penetration part of the cross section of welded sample was polished on emery papers (180, 240, 400, 600 and 800 grit), and the on velvet cloth smeared with 0.75µ alumina (Al_2O_3) slurry. The samples were ultrasonically cleaned in distilled water at each stage of polishing. To identify the fusion zone and HAZ, surface area of 50 mm X 10 mm in case of top surface and 50 mm X 3 mm in case of cross section respectively was used for electrolytic etching by ASTM standard A-262 Practice A test. In practice A, the samples were electrolytically etched in 10 wt% oxalic acid solution with current density of 1 A/cm^2 for 90 seconds. The weld penetration difference can be easily seen from figure 2 at different heat inputs. The samples were then examined under optical microscope (Zeiss Axiolab).

After etching, the geometry of welded samples was measured at different heat input conditions, which clearly differentiates the weld geometry of all the three samples. It is measured with the help of electronic vernier caliper as shown in Figure 3 and Table III. Let w = front width or weld width, r = front height or height of reinforcement and p = depth of penetration.

Figure 2 Weld penetrations at different heat inputs

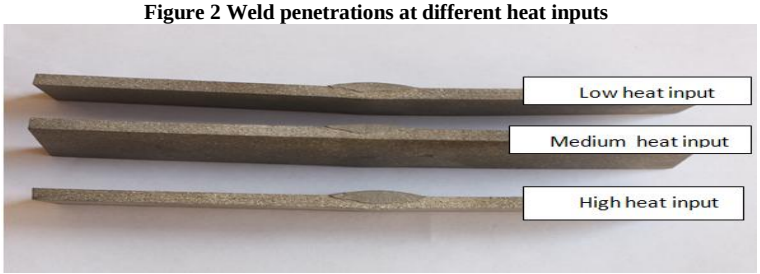

Figure 3 a) Weld bead at low heat input b) Weld bead at medium heat input c) Weld bead at high heat input d) Weld bead geometry

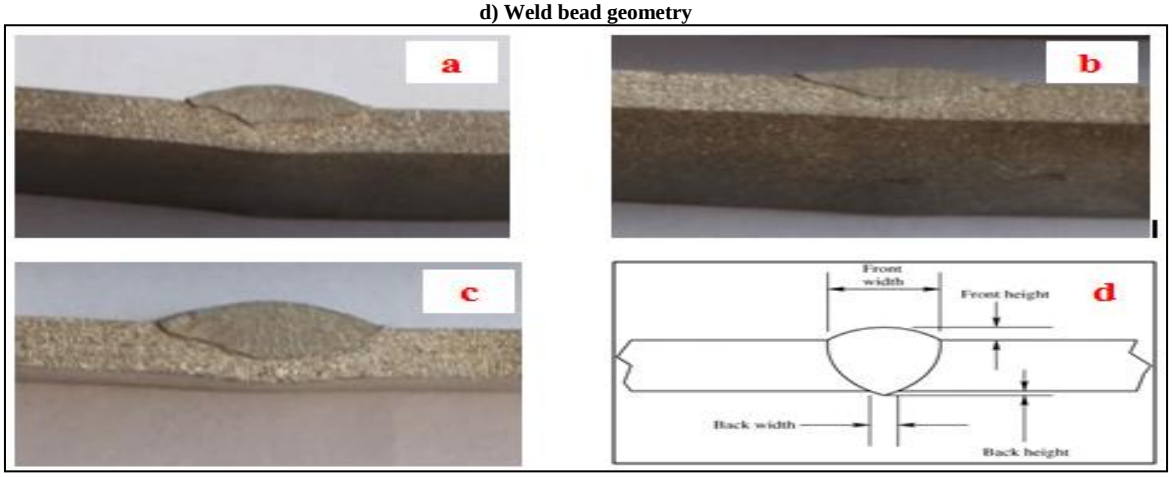

Table III Weldment characteristics at different heat input

Low heat input	Medium heat input	High heat input
w = 10.80 mm	w = 10.80 mm	w = 10.80 mm
r = 1.49 mm	r = 1.57 mm	r = 2.28 mm
p = 0.36 mm	p = 0.50 mm	p = 1.75 mm

From table III it is clear that as the heat input increases the depth of penetration increases along with the height of reinforcement. There is no affect on the weld width due to increase in heat input. Full penetration welds were obtained in all the three combinations of heat input (75A, 100A, 125A). As indicated by these values it is found that as heat input increases the fusion areas of the joints also increase proportionately. The same trend is followed for the HAZ area associated with each of these joints and also that fusion zone and HAZ area increase with increase in heat input. Optical micrographs showing the microstructures of weld zone, fusion boundary and HAZ for different heat input combinations are presented from Figure 4a & 4b, 5a & 5b, and 6a & 6b. It is observed from these optical micrographs that as heat input increases the dendrite size and inter dendritic spacing in the weld metal also increase. This dendrite size variation can be attributed to the fact that at low heat input, cooling rate is relatively higher due to which steep thermal gradients are established in the weld metal, which in turn allow lesser time for the dendrites to grow, whereas at high heat input, cooling rate is slow which provide sample time for the dendrites to grow farther into the fusion zone.

Figure 4 Optical micrographs at low heat input a) weld metal b) fusion boundary and HAZ

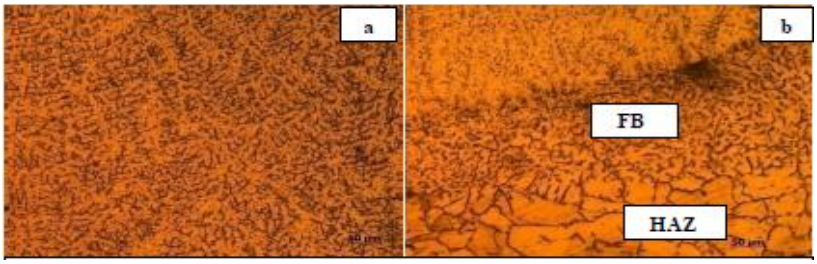

Figure 5 Optical micrographs at medium heat input a) weld metal b) fusion boundary and HAZ

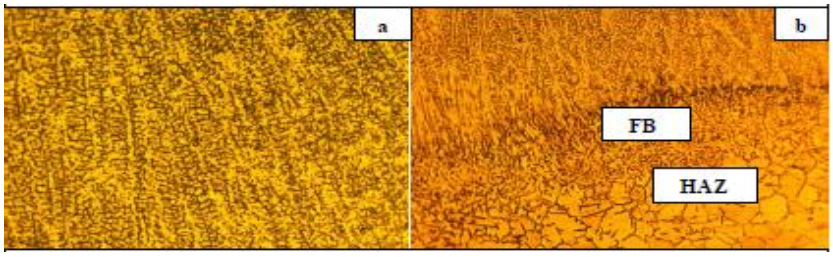

Figure 6 Optical micrographs at high heat input a) weld metal b) fusion boundary and HAZ

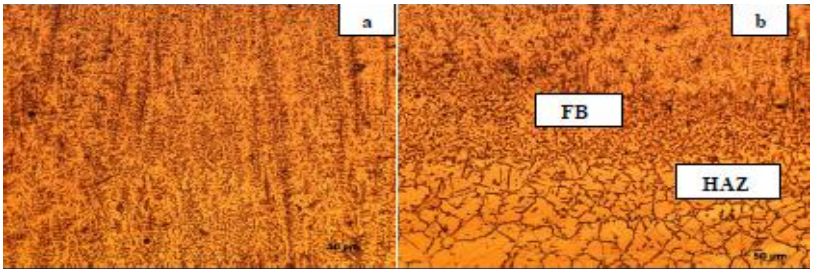

IV. Conclusions

This study comprises bead-on-plate SMAW of solution annealed plates using electrode "AWS E308L-16" of diameter 3.15 mm. Double V-groove design was used so that welding could be accomplished ensuring full penetration. From the experimental results it was confirmed that heat input had greater affect on height of reinforcement and depth of penetration and both increases with increase in heat input. There is no affect of heat input on the weld width. Fusion zone and HAZ area increase with increase in heat input. It is observed from optical micrographs that as heat input increases the dendrite size and inter dendritic spacing in the weld metal also increase. It can be attributed to the fact that at low heat input, cooling rate is relatively higher. Due to which steep thermal gradients are established in the weld metal. In turn allow lesser time for the dendrites to grow. Whereas at high heat input, cooling rate is slow which provide sample time for the dendrites to grow farther into the fusion zone.

References

[1] G. George and H. Shaikh, Corrosion of Austenitic Stainless Steels: Mechanism, Mitigation and Monitoring, ed. by H.S. Khatak and B. Raj, Wood head Publishing House, Cambridge, England, 2002.
[2] A. J. Sedriks, Corrosion of Stainless Steels, 2nd ed., J. Wiley & Sons, New York, 1996.
[3] G. Fontana, Corrosion Engineering, 3rd ed., Tata McGraw Hill Education Pvt. Ltd., New York, 2005.
[4] S.M. Bruemmer, NUREG topic report, U.S.Nuclear regulatory commission, 1989.
[5] D.M. Viano, N.U. Ahmed, G.O. Schumann, "Influence of heat input and travel speed on microstructure and mechanical properties of double tandem submerged arc high strength low alloy steel weldments", Science and Technology of Welding & Joining, vol.5(1), 2000, pp. 26-34.
[6] K. Prasad, D. K. Dwivedi , "Some investigations on microstructure and mechanical properties of submerged arc welded HSLA steel joints", International Journal of Advanced Manufacturing Technology, vol.36 (5) , 2008, pp. 475-483.
[7] K. Prasad, D. K. Dwivedi, "Microstructure and Tensile Properties of Submerged Arc Welded 1.25Cr-0.5Mo Steel Joints", Materials and Manufacturing Processes, vol. 23(5), 2008, pp. 463-468.
[8] D.M. Viano, N.U. Ahmed, G.O. Schumann, "Influence of heat input and travel speed on microstructure and mechanical properties of double tandem submerged arc high strength low alloy steel weldments", Journal of science and technology of welding and joining, vol.5, 2000, pp. 26-34.
[9] G. Karthik, P. Karuppuswamy, V. Amarnath, "Comparative Evaluation of Mechanical Properties and Micro Structural Characteristics of 304 Stainless Steel Weldments in TIG and SMAW Welding Processes", International Journal of Current Engineering and Technology, 2014, pp.200-206.
[10] P. Sathiya, S. Aravindan, P.M. Ajith, B. Arivazhagan, A. Noorul Haq, " Microstructural characteristics on bead on plate welding of AISI 904 L super austenitic stainless steel using Gas metal arc welding process", International Journal of Engineering, Science and Technology, Vol. 2(6), 2010, pp. 189-199.
[11] D. Kianersi, A. Mostafaei, A. A. Amadeh, "Resistance spot welding joints of AISI 316L austenitic stainless steel sheets: Phase transformations, mechanical properties and microstructure characterizations", Materials and Design 61, 2014, pp. 251–263.